Microdroplet formation and flow characteristics of water and nanofluids in microfluidic channel

André Filipe Loureiro Governo
andre.governo@tecnico.ulisboa.pt

Instituto Superior Técnico, Universidade de Lisboa, Portugal

November 2019

Abstract

The generation of microdroplets in a highly controllable environment such as microfluidic channels has been widely studied in the last decades due to its large interdisciplinary range of applications. However, its dynamics are not fully understood and the application of nanofluids into droplet formation has not received much attention. Within this scope, two different T-shaped channels were fabricated in polydimethylsiloxane using soft lithography methods, with different aspect ratios of 0.375 and 0.1875, and equal width ratio of 1, to be tested. The images of the experiments were acquired with a monochromatic CMOS camera, mounted on a microscope. The droplet formation process was characterized for the squeezing, transitional and dripping regimes, with a continuous phase of mineral with 1% w/w Span 80 and a dispersed phase of distilled water with w/w 0.05% fluorescent dye for Capillary numbers between 0.002 and 0.3 and flowrate ratios between 0.01 and 0.8. It was verified that the non-dimensional droplet volume increased with the flowrate ratio and aspect ratio but decreased with the Capillary number. A linear fitting was found appropriate for the squeezing regime, whereas a power-law behaviour adopted in dripping regime. Then, the addition of different concentrations of Al_2O_3 (0.01%, 0.025% and 0.1%) nanoparticles to the distilled water was studied. The droplet non-dimensional volume increased with the concentration of nanoparticles for the transitional regime but did not change significantly for the dripping regime. This was attributed to a change in the base fluid properties, specifically an increase in interfacial tension and viscosity.

Keywords: Microfluidics, T-junction, Nanofluids, Microfabrication, Microdroplets

1. Introduction

Since its advent, microfluidics has experienced an increase in its applications due to its inherent multidisciplinary character.

One of the areas of microfluidics deals with 2-phase flows, when two immiscible fluids interact in such a way that emulsions in the form of monodisperse droplets can be formed. These droplets have inumerous applications ranging from virus detection, fast analytical systems, development and screening of biological assays, the production of polymer particles, nanoparticles, in vitro compartmentalization and others [16, 20]. On the other hand, nanofluids are considered the fluids of the future. Although most of the focus of their research is based on their improvement of thermophysical properties related with heat transfer, it also has applications in MEMS and biotechnology [1, 4]. In 1995, the addition of truly nanoparticle dimensions, revolutionized this field since problems like clogging and erosion and were largely diminished [1].

Although emulsifying techniques have been around for a long time, bulk methods do not offer reproducible and controllable pattern formations. Most microdroplet generation systems are able to form monodisperse droplet sizes with polydispersity, defined as $\alpha = \frac{\delta}{d_{av}} \times 100\%$, as low as 2 % [16].

The first production of monodisperse droplets in a microfluidic T-junction was reported by Thorsen et al. [17]. They attributed the formation of droplets to a competition of shear and interfacial tension stresses:

$$r \sim \frac{\sigma}{\mu\dot{\varepsilon}} \tag{1}$$

where r is the droplet radius, and $\dot{\varepsilon}$ is the shear rate. Since then, a lot more methods have been discovered and studied. They can be divided in two types: active and passive. Droplet generation can be forced by active methods like eletric fields, piezoeletric actuators and other external driving forces [2, 20]. Oppositely, passive methods do not need any driving forces, droplets are formed mainly due to geometry and by tuning kinematic and physical properties of the fluids. Although passive methods are always preferable, active methods do offer

a more controllable and defined droplet formation, often required for LOC applications, for example [16].

Generally, it is observed that the droplet formation(size/polydispersity) process depends on [16]: flow rates of both fluids; channel dimensions; viscosities of both fluids; interfacial tension between both fluids (presence and concentration of surfactants); wettability of channel walls.

The effects from these parameters are slightly different depending on the generation mechanism used and the droplet formation regime.

Droplet generators: T-junctions

T-junctions are one of the most common techniques to achieve reproducible and controllable droplet formation.

Three different regimes of droplet formation are commonly reported in literature, depending on the continuous phase Ca: squeezing, dripping and jetting. Some authors also include a transitional regime between squeezing and dripping [7], but this is somehow controversial. Regime identification is somewhat dependent on the author's subjectivity since unique characterizing parameters are not completely established.

Droplet formation regimes

Squeezing regime is characterized by low Ca numbers, typically Ca $< 10^{-2}$ [6], where droplet detachment is dominated by a dramatic increase in pressure force upstream of the forming interface. The shear force is not strong enough to cause relevant deformation and the formed thread will grow and obstruct the channel, restricting the continuous phase flow. As the Ca number is increased, the dripping regime is attained where the shear forces exerted by the continuous phase start to play an important role in droplet formation, deforming the interface as it enters the junction. The deformation forces become high enough ensuring droplets are detached before even filling the entire channel. Once the dispersed phase thread reaches a critical size, the interfacial tension force is not strong enough to resist the elongation and the droplet detaches. It was further observed that, increasing Ca in the dripping regime, dislocates the formation zone downstream of the exit channel and away from the junction. The formation enters the jetting regime, when there is a clear development of an elongated finger, and droplet detachment occurs at the end of the jet by Rayleigh-Plateau instability. Finally, for Ca numbers large enough, paralell flow is observed and both fluids flow smoothly with a well paralelly defined interface and no droplet formation occurs. Between the squeezing and dripping regimes, it appears an intermediate regime where both shear and pressure forces share similar importance in the process, which is known as the transitional regime [3, 7].

Parameters influencing droplet formation

Droplet size can be controlled by numerous parameters, arising from microchannel design and fluid and flow properties. In order to accomplish a water-in-oil droplet formation, its very important to assure an hydrophobic surface of the microchannel walls meaning that the continuous phase (in this case, oil) should wet the channel surface favorably. Elastomers like PDMS are naturally hydrophobic. The non-dimensional droplet diameter is observed to increase with the aspect ratio Γ [8, 3] and width ratio Λ [11, 9], either by increasing the depth h, decreasing the continuous phase width W_c or increasing the dispersed phase width W_d. Altering the flowrates of both phases also affects droplet formation. Droplet size is observed to increase as the flow rate ratio increases but becomes smaller as Ca increases. In the squeezing regime, literature shows that the flowrate ratio is a dominant parameter defining droplet size, and it increases linearly with it for high confinement conditions [6]. In the dripping regime since the Ca is higher, droplet formation is less dependent on the flowrate ratio Q. Moreover, numerical data from De Menech et. al [5] shows that effect of confinement still plays a role in defining droplet size. In the dripping regime, droplet size is more influenced by Q_c, *i.e.*, Ca, than from the flowrate ratio. It is also observed that droplet size does not vary significantly for higher Ca in the dripping regime [9].

In water-in-oil emulsions, altering viscosity can be done by changing oil types, mixing water with other solutions or compounds, changing temperature, and others [3, 13, 14]. In the squeezing regime, droplet formation is verified to be independent of the viscosity ratio λ, as it does not depend significantly on the shear forces [10, 3]. In the dripping regime, its effect starts to become noticeable and it shows to have a decreasing effect on droplet size [10]. Both viscosity and interfacial tension, which play an important role in droplet formation, are temperature dependent. Murshed et. al [12] explored nanofluids and temperature dependence in droplet generation devices. The introduction of nanoparticles in the dispersed phase of a T-junction, directly affects the process by introducing a small change in viscosity and a large decrease in interfacial tension [13, 14].

Scaling laws

It is important for practical applications to be able to make this kind of predictions for a specific set of conditions.

Considering a 2-stage process of growth and neck squeezing, and arguing negligible influence of Ca on droplet size in the squeezing regime, Garstecki et. al [6] proposed a scaling law based on a linear fitting

between droplet length L and Q:

$$\frac{L}{W_c} = 1 + \frac{d_{neck}}{W_c} \times Q \quad (2)$$

where d_{neck} is the forming droplet neck diameter. The model was found to be limited to the experimental conditions from their work ($\Lambda < 0.5$, $h < W_c$ and $Ca < 0.01$). This scaling was further adapted to include a broader range of geometries, by replacing both coefficients by appropriate fitting parameters that depend on the T-junction dimensions [19]. This was found to properly relate purely squeezing conditions and indicate that this regime is mainly governed by Q and T-junction geometry.

For droplets generated in the dripping/transitional regimes, Liu et al. [11] proposed a scaling function of Ca and Q:

$$\frac{L}{W_c} = (\varepsilon + KQ) \times Ca^m \quad (3)$$

where ε, K and m are fitting parameters.

Other correlations based on force balances, step models and theoretical analysis have been proposed in literature [18, 7], yet they are not able to predict accurately results for other researchers.

The present work intends to complement the current knowledge in droplet formation dynamics, by providing data in innovative experimental conditions. The effects of controlling parameters on droplet size, in the squeezing, transitional and dripping regimes, will be studied. These parameters include the flowrate ratio Q, Capillary number of the continuous phase Ca and nanoparticle concentration. After analysis of the mechanisms involved in each regime, the results obtained for the distilled water were compared to the ones acquired for Aluminium Dioxide Al_2O_3 nanofluid.

2. Materials, experimental methods and setup

In this section, a brief explanation of the manufacture process of the T-shaped microchannels used in this work is summarized, together with a description of the experimental setup and methodologies.

2.1. Fabrication of microfluidic T-channels

The microfluidic chips containing several microchannels, like shown in figure 1 (b), were manufactured using polydimethylsiloxane (PDMS), by soft lithography.

The overall microfabrication process includes the Al coated glass hardmask by photolithography, the master by soft lithography and the microchannels by replica molding (PDMS casting). The 2D microchannels features were drawn in *AutoCAD* software and the features were printed in the thin Al film using Direct Write lithography by laser.

Shortly, the fabrication procedure consists of exposing a 75 μm thick SU-8 50 photoresist layer to UV-light through the opaque Al mask, softening the geometrical features of the microchannels geometry. An appropriate solvent is used to etch the less soluble part of the photoresist layer, creating the mold. The mold is then carefully filled with pre-PDMS elastomer using 2 PMMA plates that are taped and aligned, and allowed to cure in a oven for 1h.

The sealing of the microchannels is made with a 500 μm PDMS membrane coating through the use of oxygen plasma treatment, ensuring that the surfaces bond covalently. This provides uniform hydrophobic wetting properties of the walls. The channels are stored in a clean environment and allowed to bond for 24h, for permanent sealing.

In order to characterize the quality and finishing, a SEM (Scanning Electron Microscope) analysis was performed, examples of which are illustrated in figure 1 (c) and (d) and characteristics summarized in Table 1, where Γ is the aspect ratio of the main channel and Λ is the width ratio between the continuous and dispersed phase channels. From SEM, it is possible to verify the quality of the manufactured microfluidic devices and a well defined perpendicularity at the T-junction. The height values were obtained using a profilometer, with a maximum difference of 2.4%.

Table 1: Designed dimensions for the T-shaped microchannels. h, W_c and W_d are the height, width of continuous phase channel and width of dispersed phase channel, respectively.

Microchannel	h (μm)	W (μm)	Γ	Λ
T1	75	224	0.335	1
T3	75	427	0.176	1

2.2. Experimental setup and methods

The setup arrangement for the experiments involves both the preparation of the working fluids and the necessary equipments. A schematics of the setup is shown in figure 2.

The DIW and aqueous nanofluids were made fluorescent by adding 0.05 % w/w of fluorescein sodium salt (*Sigma-Aldrich*). The connection from the syringes was made through polyethylene (PE) BTPE-90 tubing and 20-ga luer locks from *Instech*. Before pumping both fluids, the microchannels were first primed with the continuous phase liquid for 15 min. After this time, the pump is stopped and the dispersed phase is turned on. When it reaches the T-junction, the continuous phase is started again. An equilibration time is needed inbetween flowrate variation, so the pressure in the channels is stabi-

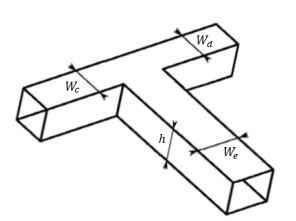

(a) Schematic representation of the T-shaped channels geometry. used in this work. Figure adapted from [15].

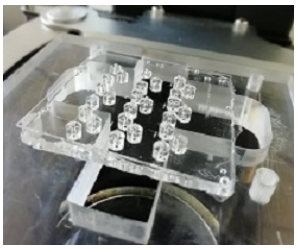

(b) Manufactured T-junction microchannels ready to be used.

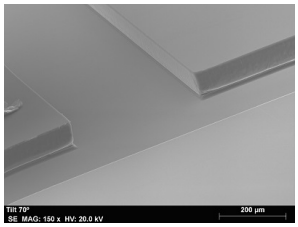

(c) 150x magnification obtained from SEM analysis of the T3 geometry.

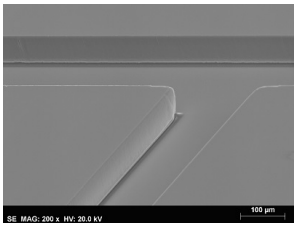

(d) 200x magnification obtained from SEM analysis of the T1 geometry.

Figure 1: Characterization of the T-junction microchannels manufactured and tested in this work.

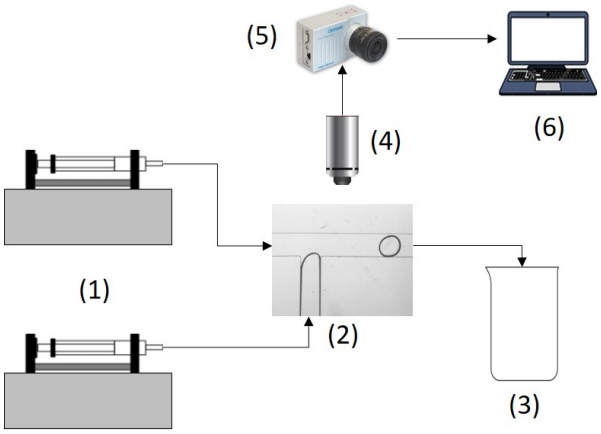

Figure 2: Experimental setup schematics. The dispersed and continuous phases are pumped by two separate syringe pumps (1) into the T-shaped microchannels (2), and the exit segment channel is connected to a deposit beaker (3). The microscope (4), which is connected to the CMOS camera (5), illuminates and captures the the amplified images, which are recorded by the camera and then exported for the working computer (6).

lized. For calculations, at least 10 droplets were measured and then averaged, in order to get a better single value for a specific regime and allow the calculation of the polydispersity index. The preparation of nanofluids involved a two-step method. It was used aluminum oxide Al_2O_3 nanofluid from *Sigma Aldrich* with a nanoparticle content of 20 ± 1 mass %. According to the manufacturer, the size of nanoparticles is 30 nm, and this is assumed as true for this work. The experimental determination of the mass of nanoparticles m_{np} and the mass of base fluid m_{np}, was based on the following equation for mixtures:

$$\phi = \frac{\frac{m_{np}}{\rho_{np}}}{\frac{m_{np}}{\rho_{np}} + \frac{m_{bf}}{\rho_{bf}}} \times 100 \tag{4}$$

where ϕ is the nanoparticle volume percentage (%), m_{np}, ρ_{np}, m_{bf} and ρ_{bf} are the mass and density of nanoparticle and base fluid, respectively. A proper dispersion was obtained by using the magnetic stirrer (Rotilabo MH15, *Carl Roth Gmbh*) and an ultrasonic homogenizer (UP200Ht, *Hierschel Ultrasonics*). Before removing the nanofluid for dilution, it was placed in the magnetic stirrer for 20 minutes for homogenization. Then, the correct volume was measured in a beaker and dilluted with DIW, to get the correct nanoparticle content in volume %. The mixture was then subjected to ultrasonication, at 60 % amplitude for 15 min in continuous mode operation. The sample was allowed to cool down at room temperature and then its properties were measured.

The dynamic viscosity was measured using a viscometer (*LVDV-II+Pro* set, *Brookfields Engineering*). The viscometer was calibrated by measuring the DIW viscosity at room temperature. The measured dynamic viscosities are presented in figure 3 (a). On the other hand, the interfacial tension was measured using the *Attension Theta* optical tensiometer. Besides calculating the interfacial tension, it was also verified the wetting properties of the PDMS material of the microchannels. For this purpose, the sessile drop method was used to calculate the static contact angle of both the distilled water and mineral oil. The results for the static contact angle of DIW and mineral oil, after averaging for three different volume drops, were 110.35 and 44.60 degrees, respectively. The interfacial tension between both liquid phases was calculated using the pendant drop method. The data obtained for the interfacial tension measurements of the nanofluid dispersions is plotted in figure 3 (b). An increase of σ is observed for all the concentrations tested. Although this is not a usual trend, similar results for surface tension of Al_2O_3 diluted nanofluids were previously published [21].

The complete characteristics of the working fluids are displayed in table 2.

3. Digital image processing

In order to obtain the droplet volume, it is necessary to analyze the 2D droplet shape images captured during the experiments. The channel geometries fabricated have aspect ratio $\Gamma < 0.335$, so, in

Table 2: Physical properties of continuous and dispersed phase fluids used for this work. The Capillary number Ca shown in the table, as before, without subscript, refers to the Ca of the continuous phase fluid Ca_c.

Fluids	Viscosity μ (mPa.s)	IF σ (mN/m)	Density ρ (Kg/m^3)
Mineral oil 1% Span 80	24.7	–	860
DIW 0.05 % fluorescent dye	0.85	5.26	973.44
DIW 0.01 vol. % Al_2O_3	0.96	5.71	-
DIW 0.025 vol. % Al_2O_3	0.99	6.23	-
DIW 0.1 vol. % Al_2O_3	1.07	6.86	-

Figure 3: Measured physical properties of the working fluids.

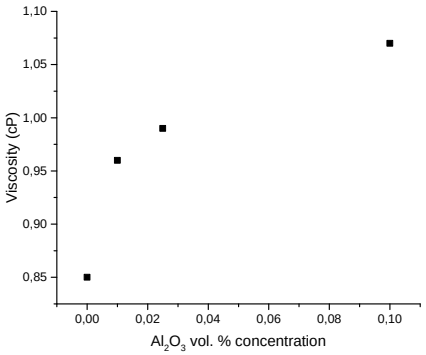

(a) Measured dynamic viscosity as a function of the vol. % concentration of Al_2O_3.

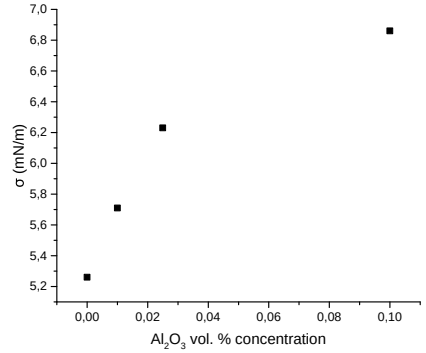

(b) Interfacial tension measurements for the Al_2O_3 dilute nanofluid for different concentrations in volume %.

the squeezing regime, where L > h, a reasonable assumption is that the slug almost fully occupies the section, in the height direction, and smooth side curvature is obtained due to interfacial tension, so it will look like a disk. For these cases, the the 3D volume is reconstructed from the 2D image from the following expression [18]:

$$V = hA - \frac{h^2 P}{2}\left(1 - \frac{\pi}{4}\right) \quad (5)$$

where A and P are the 2D area and perimeter of a single droplet, respectively, and h is the channel height. This equations accounts for the total volume occupied by the length of the droplet and subtracts the volume associated with the side curvatures, by assuming these last equal to $\frac{h}{2}$ and that the droplet is perfectly symmetrical to the center of the microchannel. In the dripping regime, if L < h is observed, the equation for the volume of a sphere with L = d is used. As with most edge detection routines, this code works by isolating the droplets in a binary image and calculating the 2D area, in pixels, and converting it into volume and length by appropriate dimension transformations. The original image is subjected to a binarization by thresholding or intensity-gradient methods, allowing the detection of the droplets boundaries.

4. Presentation and Discussion of the Results

In this section, the results regarding the study on the droplet formation parameters in a T-junction, with DIW and Al_2O_3 aqueous nanofluid as the dispersed phase and mineral oil as continuous phase, are going to be presented. For each T-channel, the experiments performed with different flowrate ratio Q, Capillary number Ca and Γ are those presented in table 3. The densities for the nanofluids were not calculated since the density ratio is almost equal to 1 for liquid-liquid droplet formation.

Table 3: Parameters to be varied in the experimental tests.

Exp. parameter	Range values
Q	0.01 - 0.8
Ca	0.002 - 0.1
Γ	0.176 and 0.335

4.1. Distilled water droplet formation

Influence of the flowrate ratio:

Experimentally, changing flowrate ratio meant changing the dispersed phase flowrate Q_d, while keeping the continuous phase Q_c constant, accord-

ing to the parameters and fluid properties measured.

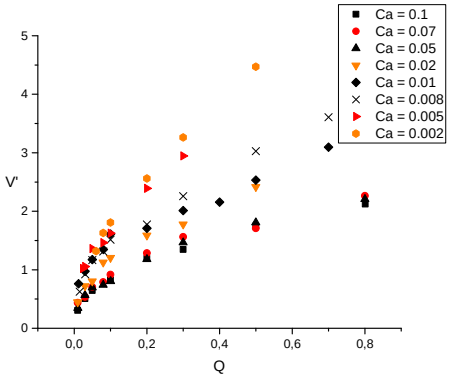

(c) Γ = 0.335

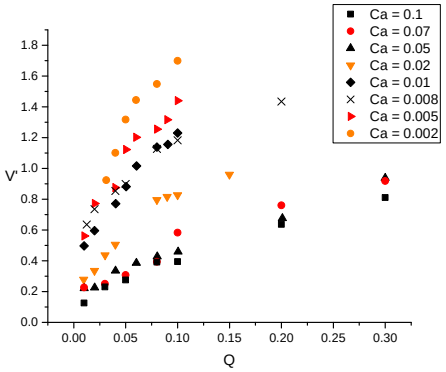

(d) Γ = 0.176

Figure 4: Variation of the dimensionless droplet volume V'= V/W_c^2h as a function of the flowrate ratio $Q=Q_d/Q_c$, for different Ca and for both geometries

The results displayed in figure 4 clearly evidence that the non-dimensional droplet volume V' increases, for all the Ca and geometries tested, with the flowrate ratio Q. It is possible to detect the existence of a change in regime from this type of graph, since one can clearly notice a decreasing variation of V' on Q, as the Ca of the continuous phase reaches higher values. This is associated with the change of regime from squeezing to transitional and dripping regimes, as the Ca is increased from 0.002 to 0.1.

In both geometries, a purely squeezing regime was observed for Ca < 0.008, whereas the dripping regime was verified for Ca > 0.02, in both geometries. Snapshots of the squeezing regime at the T1 geometry are depicted in figure 5. In the squeezing regime, the forming DIW interface is observed to grow freely because the mineral oil flowrate is very small and the tangential shear forces exerted are not sufficient to deform it before it fills the entire channel. As it grows, the interface restricts the continuous phase fluid path through the small gaps

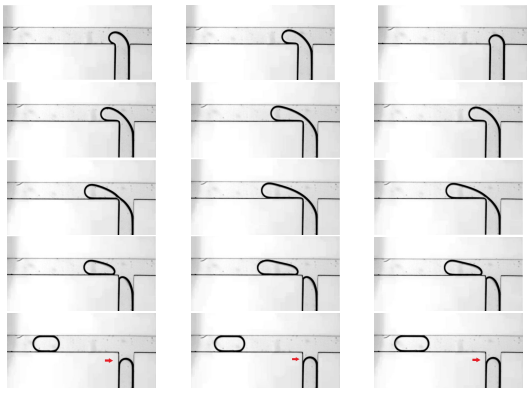

Figure 5: Droplet formation process in the squeezing regime for Q = 0.06, 0.08 and 0.1 (left to right), at Ca = 0.002, for the T1 geometry.

around it, reducing the available flow area with the consequence being an increase of the static pressure upstream. The pressure difference established downstream and upstream of the attached thread, creates a strong necking force at the interface, which is the inducing break-up factor. After detachment, the thread is noted to recede a small distance into the dispersed phase channel, which is visible in the last 2 pictures from figure 5, indicated with a red arrow.

This lag mechanism was also studied by Glawdel et. al [7] for the transitional regime and is here further extended to the squeezing regime, for small flowrate ratio Q and aspect ratio Γ conditions. It is also observed that the interface always ruptures at the T-junction. Considering the 2-stage linear scaling law proposed by Garstecki et al. [6] (see equation 2) for the squeezing regime, the data for Ca = 0.002 and Ca = 0.005 seems to find reasonable agreement to the function V' = 0.95 + 7.2Q (R^2=0.9919) - see figure 6 (a). Interestingly, data obtained for the T3 geometry does not correlate well with this fitting - 6 (b). Most likely, this is related to a distinct pressure difference behaviour obtained between upstream and downstream sides of the protruding thread, in different aspect ratio geometries.

On the other hand, in the dripping regime, the effect of the upstream pressure forces start to become less significant and shear stress exerted on the interface gains the role of the dominant detachment mechanism, with the increase of Q_c. Contrary to the squeezing regime, the dispersed phase thread does not fill the entire main channel due to the higher shear forces exerted during the growth stage, which causes it to deform apreciably as soon it reaches the T-junction, as it is seen in figure 7.

This causes the thread to rupture more rapidly, creating smaller droplets in a high formation fre-

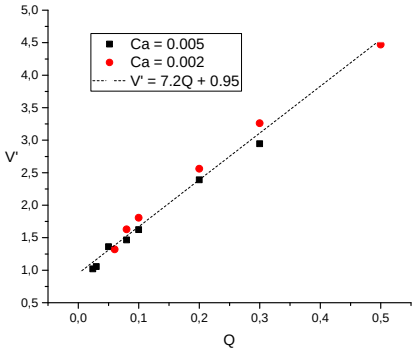

(a) Γ = 0.335

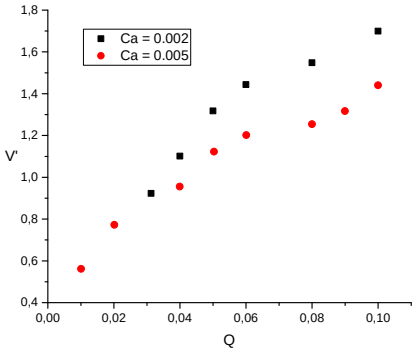

(b) Γ = 0.176

Figure 6: Variation of the droplet dimensionless volume V' with the flowrate ratio Q, at constant Ca in the squeezing regime for both geometries.

quency. The increase of V' with Q, in this regime, is less pronounced than that of the squeezing regime and a power-law was observed to be the best fitting for the data obtained, as observed in figure 8.

Although researchers discuss about a critical Ca for regime change between squeezing, dripping and jetting, the evolution between the first two is gradual and a transitional regime is usually verified. In this work, the transitional regime was verified for $0.008 \leq Ca \leq 0.02$.

Influence of the Capillary number Ca:

The influence of Ca on droplet volume was studied by maintaining a constant flowrate ratio Q and a constant dispersed phase flowrate Q_d. The results are plotted in figures 9 and 10.

The droplet V' was found to decrease with Ca for most of the flowrate ratios tested and a power-law behaviour is verified for both geometries. The exponent seems not to vary much for the T1 geometry, while for the T3 geometry, a change in slope is observed for Ca = 0.01 accompanied by a change in the exponent of the power law, which is not clearly observed in the T1 geometry. Furthermore, the

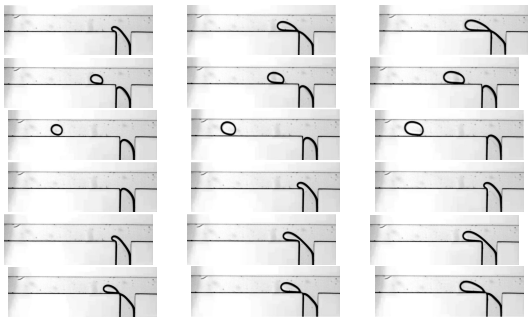

Figure 7: Droplet formation process in the dripping regime for Q = 0.01, 0.03 and 0.1 (left to right), at Ca = 0.1, for the T1 geometry.

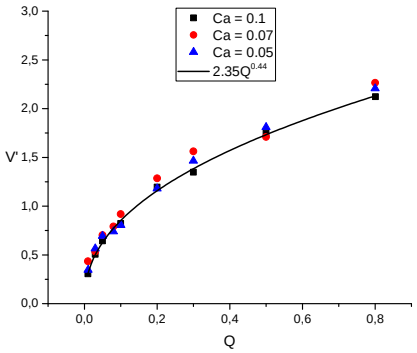

(a) Γ = 0.335

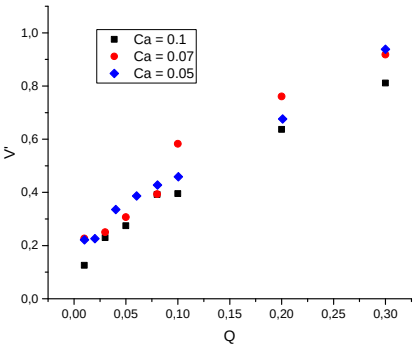

(b) Γ = 0.176

Figure 8: Variation of the droplet dimensionless volume V' with the flowrate ratio Q, at constant Ca in the dripping regime for both geometries.

change in the fitting coefficient from $V' \propto Ca^{-0.25}$ to $V' \propto Ca^{-0.45}$ shows that Ca is a more influential parameter in the dripping regime as it has a more steeper decreasing change, whereas in the T1 geometry, the effect of confinement is more dominant and the Ca influence is not so clear.

When the effect of the dispersed phase flowrate Q_d is considered in figure 10, it is observed that

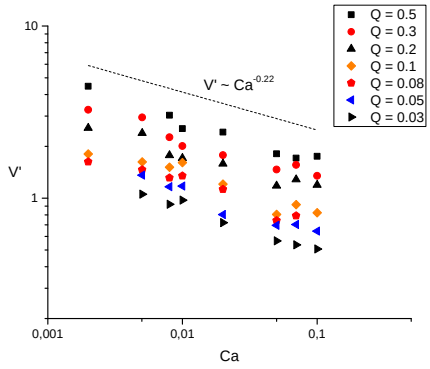

(a) $\Gamma = 0.335$

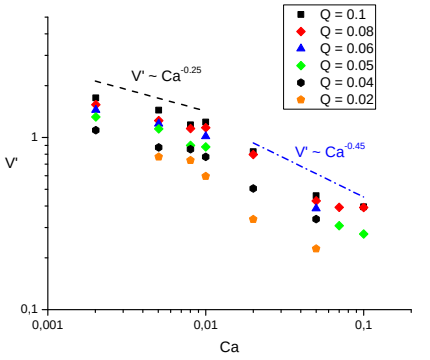

(b) $\Gamma = 0.176$

Figure 9: Variation of the dimensionless droplet volume V' with Ca for different Q and for both geometries.

this parameter has a much more strong influence on the droplet V' than the flowrate ratio Q. The exponential fitting parameter is increased (in absolute terms) to -0.62.

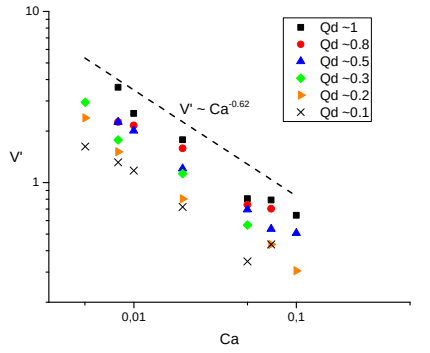

Figure 10: Variation of the dimensionless droplet volume V' with Ca for different Q_d and T1 geometry.

For the transitional regime, since both forces share similar importance in the process, this physical description is also not so clear but similar comparisons are checked. It is therefore concluded that a low aspect ratio Γ does have a strong impact on the droplet size and it should be taken into account, specially for high Ca numbers.

4.2. Aqueous Al_2O_3 nanofluid droplet formation

The influence of the addition of nanoparticles to the dispersed phase base fluid of DIW with 0.05 % w/w fluorescent dye was studied. Three different volume % concentrations of Al_2O_3 nanoparticles - see table 3 - were added and tested in the T1 geometry, for the same conditions of flowrate ratio and continuous phase flowrate Q_c, corresponding to dripping and transition regimes.

Because the flowrates Q_c and Q_d were kept the same, different droplet volumes are expected since there is a non negligible variation of fluid properties affecting droplet formation. The interfacial tension between phases and the viscosity were found to increase with the addition of Al_2O_3 nanoparticles - figure 3. Besides these two properties sharing distinct effects on droplet formation, they also share different importance, depending on the regime. In figure 11, the dimensionless droplet volumes V' are plotted against Q, for constant Ca of the continuous phase.

From the results data, at Ca = 0.1 (Figure 11 (a)), it is not observed a notorious deviation of the values of V' relative to the base fluid ones (0% Al_2O_3). The non-dimensional droplet volumes, for 0.1% concentration of Al_2O_3, are observed to match closely to the ones for DIW, while, for the lower concentrations, it seems to slightly reduce in comparison with the previous two. However, for smaller values of the continuous phase Ca, specifically Ca = 0.01 (Figure 11 (b)), V' increases with the concentration of Al_2O_3 nanoparticles for most of the conditions. The maximum increase of V' in comparison with the value from the base fluid was obtained for Ca = 0.01, a concentration of 0.1% and Q = 0.01, as 38%.

Influence of the concentration of Al_2O_3 nanoparticles

As it was noted, as the Ca number is increased, the influence of the addition of Al_2O_3 nanoparticles is noted to decrease, and the difference, comparatively to the values obtained for DIW, shortens. This can easily be visualized if we plot the variation of V' with the different concentration of nanoparticles, as it is shown in figure 12.

The non-dimensional droplet volumes, for Ca = 0.01 and Ca = 0.02, display a growing variation with the addition of Al_2O_3 nanoparticles, for most of the cases. However, for Ca = 0.05, this trend is

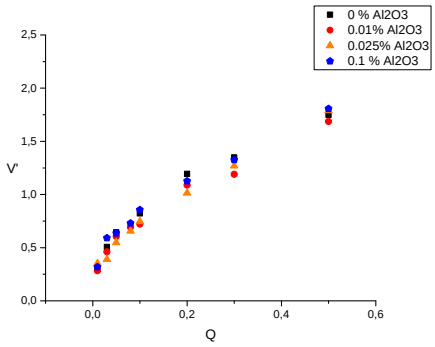

(a) Ca = 0.1

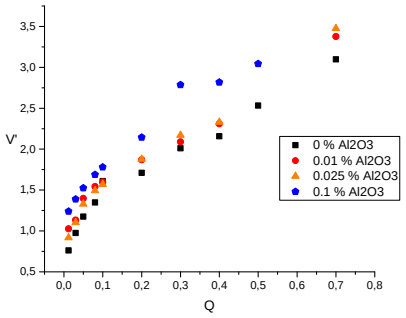

(b) Ca = 0.01

Figure 11: Variation of the dimensionless droplet volume V' as a function of the flowrate ratio Q, for different vol. % of nanoparticles in the dispersed phase and for different Ca.

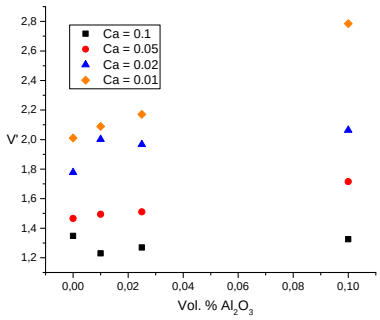

(a) Q = 0.3

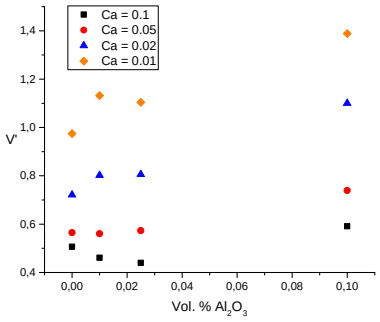

(b) Q = 0.03

Figure 12: Variation of the dimensionless droplet volume V' as a function of vol. % concentration of nanoparticles in the dispersed phase, for constant Q and for different Ca.

not strictly observed while for Ca = 0.1, the values of V' actually slightly reduce.

From this analysis, it is plausible to argue that distinct phenomenon must be at play for the several Ca condition that influence nanofluid droplet volume differently.

The increase of the viscosity ratio (by means of an increase of the dispersed phase viscosity μ_d), with the addition of nanoparticles, is expected to influence droplet V' by affecting the shear forces exerted at the thread interface. However, the effect of μ_d is expected to be negligible when compared with the one from μ_c, that remains constant and much greater than the former. Furthermore, an increase in μ_d is also added in terms of the friction resistance at the disperse phase fluid thread and stronger streamwise forces will then be required to push the same volume of dispersed phase fluid. This has similar implications as the increase of the interfacial tension with nanoparticle concentration, because this leads to a stronger interface, less prone to detachment. These remarks might explain why the values of V' for the dripping regime, at Ca = 0.1, do not differ much with the addition of nanoparticles, while the values for the transitional regime, specially at Ca = 0.01, notoriously increase comparatively to the ones obtained for DIW.

The trend of the results appears to show that the reduction of Ca makes the V' variation with the % concentration of Al_2O_3 to be more pronounced. Apart from the changes in the physical properties for the nanofluids, no other justification could be made for such observations regarding droplet volume.

5. Conclusions

A thorough analysis of distilled water droplet formation characteristics was performed by employing 8 diferent Ca (0.002-0.1) and flowrate ratios Q (0.01-0.8) conditions for both geometries. Furthermore, the application of different concentrations of Al_2O_3 to the base DIW dispersed phase was carried out.

The squeezing regime, occurring for Ca $\leq$ 0.005, was found to be strongly dependent on the flowrate ratio, and a linear fitting proved to represent the

data accurately for the T1 geometry. With the increase of the Ca, the transitional regime was attained and the non-dimensional droplet volume V' is expected to be dependent on both Q and Ca in this regime, which made droplet volume predictions difficult. At Ca $\geq$ 0.05, dripping regime was achieved and formed droplets showed minor variations in V' with Q. Data was accurately fitted to a power-law behaviour, with an exponent of 0.44. Regarding the influence of the continuous phase, it was observed a decrease of V' with Ca, for all conditions. However, an higher dependence of V' on Ca was noted, with constant dispersed phase flowrate Q_d, and a power-law equation with an of -0.62, accurately represented the data. Finally, a study of the influence of the aspect ratio showed that V' decreased with it. Interestingly, this effect was observed to be more pronounced in the dripping regime.

The addition of Al_2O_3 nanoparticles to the distilled water phase in the droplet generator was observed to promote an increase of V' in the transitional regime, whereas for the dripping regime the influence was negligible as the data practically coincide for the different studied concentrations. This was attributed to the change of properties, since it was observed that both interfacial tension and viscosity increased with % of Al_2O_3 nanoparticles. A successful utilization of nanofluids in microchannel devices and as dispersed phase fluid for the formation of monodisperse droplets was obtained. This topic still requires further studies as applications of nanofluids for micro-sized flow channels and devices have promissing future in important applications.

References

[1] A. Choi, S. U. S.; Eastman. Enhancing thermal conductivity of fluids with nanoparticles. *Proceedings of the 1995 ASME International Mechanical Engineering Congress and Exposition*, 66(March):99–105, 1995.

[2] G. F. Christopher and S. L. Anna. Microfluidic methods for generating continuous droplet streams. *Journal of Physics D: Applied Physics*, 40(19):319–336, 2007.

[3] G. F. Christopher, N. N. Noharuddin, J. A. Taylor, and S. L. Anna. Experimental observations of the squeezing-to-dripping transition in T-shaped microfluidic junctions. *Physical Review E - Statistical, Nonlinear, and Soft Matter Physics*, 78(3):1–12, 2008.

[4] S. K. Das, S. U. Choi, and H. E. Patel. Heat transfer in nanofluids - A review. *Heat Transfer Engineering*, 27(10):3–19, 2006.

[5] M. De Menech, P. Garstecki, F. Jousse, and H. A. Stone. Transition from squeezing to dripping in a microfluidic T-shaped junction. *Journal of Fluid Mechanics*, 595:141–161, 2008.

[6] P. Garstecki, M. J. Fuerstman, H. A. Stone, and G. M. Whitesides. Formation of droplets and bubbles in a microfluidic T-junction - Scaling and mechanism of break-up. *Lab on a Chip*, 6(3):437–446, 2006.

[7] T. Glawdel, C. Elbuken, and C. L. Ren. Droplet formation in microfluidic T-junction generators operating in the transitional regime. I. Experimental observations. *Physical Review E - Statistical, Nonlinear, and Soft Matter Physics*, 85(1):1–9, 2012.

[8] A. Gupta and R. Kumar. Effect of geometry on droplet formation in the squeezing regime in a microfluidic T-junction. *Microfluidics and Nanofluidics*, 8(6):799–812, 2010.

[9] A. Gupta and R. Kumar. Flow regime transition at high capillary numbers in a microfluidic T-junction: Viscosity contrast and geometry effect. *Physics of Fluids*, 22(12):1–11, 2010.

[10] H. Liu and Y. Zhang. Droplet formation in a T-shaped microfluidic junction. *Journal of Applied Physics*, 106(3):1–20, 2009.

[11] H. Liu and Y. Zhang. Droplet formation in microfluidic cross-junctions. *Physics of Fluids*, 23(8):1–12, 2011.

[12] S. Murshed and N.-T. Nguyen. *Nanofluids: Synthesis, Properties and Applications. Nanofluids in droplet-based microfluidics*. Nova Science Publishers, Inc., 2014.

[13] S. M. S. Murshed, S. H. Tan, and N. T. Nguyen. Temperature dependence of interfacial properties and viscosity of nanofluids for droplet-based microfluidics. *Journal of Physics D: Applied Physics*, 41(8):1–5, 2008.

[14] S. M. S. Murshed, S. H. Tan, N. T. Nguyen, T. N. Wong, and L. Yobas. Microdroplet formation of water and nanofluids in heat-induced microfluidic T-junction. *Microfluidics and Nanofluidics*, 6(2):253–259, 2009.

[15] D. Sampaio. Caracterização experimental da camada de plasma em escoamentos de sangue animal no interior de microcanais com promotores de mistura em zigzag. MSC thesis. Mechanical Engineering Department, Instituto Superior Tecnico, University of Lisbon,. 2016.

[16] R. Seemann, M. Brinkmann, T. Pfohl, and S. Herminghaus. Droplet based microfluidics. *Reports on Progress in Physics*, 75:1–41, 2012.

[17] T. Thorsen, R. W. Roberts, F. H. Arnold, and S. R. Quake. Dynamic pattern formation in a vesicle-generating microfluidic device. *Physical Review Letters*, 86(18):4163–4166, 2001.

[18] V. Van Steijn, C. R. Kleijn, and M. T. Kreutzer. Predictive model for the size of bubbles and droplets created in microfluidic T-junctions. *Lab on a Chip*, 10(19):2513–2518, 2010.

[19] J. H. Xu, S. W. Li, J. Tan, and G. S. Luo. Correlations of droplet formation in T-junction microfluidic devices: From squeezing to dripping. *Microfluidics and Nanofluidics*, 5(6):711–717, 2008.

[20] L. I. U. Zhao-miao, Y. Yang, D. U. Yu, and P. Yan. Advances in droplet-based microfluidic technology and its applications. *Chinese Journal of Analytical Chemistry*, 45(2):282–296, 2017.

[21] D. S. Zhu, S. Y. Wu, and N. Wang. Surface tension and viscosity of aluminum oxide nanofluids. *AIP Conference Proceedings*, 1207:460–464, 2010.